



A Comparative Study of Structure, FMR and Magnetic Properties of 80%Mg [Fe] ₂O₄- 20%Ba [Fe] ₁₂O₁₉as Nanocomposite and Mixture Ferrites

R.E. El-Shater^{1*}

¹ Physics Department, Faculty of Science, Tanta University, Tanta 31527, Egypt

ABSTRACT

Received 25th July 2019
Accepted 16th Dec. 2019

This investigation presents a design of 20% M-type BaFe₁₂O₁₉ hexaferrite as a core coated by 80% MgFe₂O₄ spinel ferrite as a shell ([Mg] ₈₀-H₂₀) in addition to, a mixture of 80% MgFe₂O₄ spinel ferrite and 20% M-type BaFe₁₂O₁₉ hexa-ferrite powders. The spinel and nanocomposite ferrite materials were synthesized by using the wet mechano-chemical co-precipitation route. All prepared samples; spinel, nanocomposite and mixture are annealed at 1200 oC for 6 hours. The results of X-ray diffraction patterns, TEM images and the transmitted IR spectra revealed the formation of two different composite materials. The results of ferromagnetic resonance FMR spectra and magnetic hysteresis loops represents contrast between the nanocomposite structure and the mixed material of the same constitutes with the same ratio

Keywords: Nanocomposites; FMR; Magnetic properties.

Introduction

Nanotechnology The discovery of ferrite materials and their derivatives created a growing interest in their preparation and characterization to meet the increasing needs for high density magnetic recording media, permanent magnets and high frequency devices with low cost. They have induced a considerable attention for active research toward fabrication of new ferrite materials with suitable properties for different applications[1]. The nanoferrites were extensively studied for their magnetic, optical, electric, elastic, vibrational and thermal properties, which are different as compared to their bulk counterparts. Values of magnetic properties of nanomaterials such as saturation magnetization, coercivity, anisotropy field, initial and maximum permeability, and squareness (saturation to remnant magnetization ratio) are important in determining their suitability for applications in specific magnetic and

electromagnetic devices. The lowest magnetic loss and high resistivity are the most needed properties for application of these ferrite materials [2].

M-type BaFe₁₂O₁₉hexa-ferrite is a hard permanent magnetic material and studied more than various M-type MFe₁₂O₁₉hexa-ferrites (M = Sr, Ba or Pb) due to its high chemical stability, saturation magnetization, coercivity and large magneto-crystalline anisotropy [3]. Spinel ferrites have the formula MFe₂O₄ where M is a divalent metal and Fe has trivalent valence. They are soft magnetic materials having low coercivity and high resistivity, which leads to applications in many fields. The cubic MgFe₂O₄ ferrite is a partially inverse spinel ferrite, where its inversion degree is sensitive to the sample structure, cation distribution, thermal treatment and preparation method [4-6]. Ferrite composites composed of both soft spinel and hard hexaferrite are promising for

excellent permanent magnets because of their low cost, high electric and corrosion resistance and relatively high Curie temperature. Their grain shape and size, crystallite size distribution and relative orientations of crystallites are difficult to quantify and control. These parameters are very important to investigate the exchange spring principle in the hard-soft ferrites [7][8]. The nanocomposites were prepared by mixing the individual components of $\text{BaFe}_{12}\text{O}_{19}$ hexaferrite and spinel $\text{Ni}_{0.8}\text{Zn}_{0.2}\text{Fe}_2\text{O}_4$ ferrites at appropriate ratio and subsequent heat treatment. The magnetization of nanocomposites showed hysteresis loops characteristic of the exchange spring system [8].

The core-shell nanoparticles of CoFe_2O_4 and CoFe_2 [9] were prepared by reducing nanoparticles of CoFe_2O_4 under hydrogen atmospheres. The magnetic data indicated coupling between the core and shell through the exchange-spring mechanism, whereas the critical thickness of the soft phase (shell) was estimated to be 8.0nm. The hysteresis loops were measured in the range of 10 – 300Oe. The exchange coupling among the core-shell structure was found to vary with the shell thickness. A phenomenological model which takes into account the thickness of disordered layer at the core-shell surface was used for determining the exchange-bias anisotropy constant K_{EB} (0.22 erg/cm^2) [10]. The magnetic nanocomposite of $\text{SrFe}_{12}\text{O}_{19}$ and $\text{Ni}_{0.7}\text{Zn}_{0.3}\text{Fe}_2\text{O}_4$ powders was prepared by dispersing the prepared $\text{SrFe}_{12}\text{O}_{19}$ nanoparticles in the mixed solution of spinel precursors. The resulted nanocomposites were annealed at 600°C for 1h. The microstructural and magnetic studies exhibited strong exchange coupling and dipolar interactions in tuning the magnetic properties of the nanocomposites [7].

The ferromagnetic resonance (FMR) of a ferrite is important for investigating the magnetic properties of magnetic materials at high frequency because the resonance originates from the interaction between nuclear spin and electromagnetic waves [11]. The FMR experiment measures the derivative of the absorbed power as a function of the applied magnetic field. The higher intensity of integrated FMR line giving the absorption spectra represents a higher magnetization. Both Lorentzian and Gaussian functions are commonly used to fit the absorption spectra. [12][13].

The aim of this research is to suggest a design for structure of nanoferrites using the hard magnetic M-type hexa-ferrite and soft spinel nanoferrite by the co-precipitation route. The XRD, TEM, FT-IR, FMR and VSM techniques are used to examine the materials.

2- Experimental

2.1 Preparation of M-type $\text{BaFe}_{12}\text{O}_{19}$ hexanoferrites

The magnetic M-type hexaferrite nanoparticles were synthesized using sol-gel self-propagation method. Proportion amounts of $\text{Ba}(\text{NO}_3)_2 \cdot 6\text{H}_2\text{O}$ and $\text{Fe}(\text{NO}_3)_3 \cdot 9\text{H}_2\text{O}$ were dissolved in deionized water and mixed under stirring. According to the molar ratio of total metal ions to citric acid ($\text{C}_6\text{H}_8\text{O}_7 \cdot \text{H}_2\text{O}$) to be unity, the citric acid was dissolved in the above solution as 1:1.

The pH of mixed solutions was constantly monitored as ammonia solution was added drop-wise until $\text{pH} \approx 9$. The sol was subsequently heated until formation and then auto combustion of the gel on a hot plate. Then, the resulted material was annealed at 1200°C for 2 h and ground to fine powder in an agate mortar. The formation of M-type hexa-nanocomposite was examined utilizing X-ray diffraction.

2.2 Preparation of cubic spinel MgFe_2O_4 nanoferrite

Proportion amounts of metallic salts; $\text{Mg}(\text{NO}_3)_2 \cdot 6\text{H}_2\text{O}$ and $\text{Fe}(\text{NO}_3)_3 \cdot 9\text{H}_2\text{O}$ were dissolved separately in deionized water under mechanical stirring for 20 minutes. The solutions were mixed under stirring for 20 minutes, and then NaOH solution was added drop wise to the mixture up to $\text{pH} \approx 10.5$. The mixed solution was heated at 80°C for two hours under stirring till the co-precipitation occurs. The precipitates were washed many times by deionized water to avoid the unwanted residuals. Thereafter, the samples were dried at 100°C for 24 hours. The dried sample was annealed at 1200°C for 6 hours in the normal atmosphere, cooled to room temperature and ground to fine powder in agate mortar.

2.3 Preparation of the nanocomposite ferrite

The nanocomposite ferrite material was prepared by the simple co-precipitation method as mentioned above except the following step: After mixing the solutions of $\text{Mg}(\text{NO}_3)_2 \cdot 6\text{H}_2\text{O}$ and $\text{Fe}(\text{NO}_3)_3 \cdot 9\text{H}_2\text{O}$ for 20 minutes, the previous prepared hexaferrite $\text{BaFe}_{12}\text{O}_{19}$ were dispersed in

the mixed solution with mass ratio of 80% of MgFe_2O_4 to 20% of $\text{BaFe}_{12}\text{O}_{19}$ under mechanical stirring, then NaOH solution was added drop wise up to PH was as 10.5. The dried samples were ground and annealed at 1200°C for 6 hours in the normal atmosphere and cooled to room temperature.

2.4 Preparation of mixed composite material

The nano-composite was prepared by mixing a weight of 80% of as-prepared spinel MgFe_2O_4 nanoferrite material with weight 20% of the sintered $\text{BaFe}_{12}\text{O}_{19}$ hexaferrite material. As-prepared nano-composite was ground for 2 hours continuously before firing in the furnace at 1200°C for 6 h in the normal atmosphere. The nano-composite material was ground to fine powder in an agate mortar.

2.5 Sample characterization

The sample characterization was carried out by a computerized GNR APD 2000 Pro X-ray diffractometer step scan type and $\text{CuK}_{\alpha 1}$ radiation with wavelength $\lambda = 1.540598 \text{ \AA}$. The lattice constant a of the cubic spinel ferrite was determined by the equation; $a = d(h^2 + k^2 + l^2)^{1/2}$, where d is the inter-planer distance calculated by Bragg's law; $2d \sin \theta = n\lambda$, where θ is the diffraction angle. The lattice constants a and c of the hexa-ferrites were calculated [14 -16];

$$\frac{1}{d_{hkl}^2} = \frac{3}{4} \left(\frac{h^2 + hk + k^2}{a^2} \right) + \frac{l^2}{c^2}$$

$$a = \left[\frac{4}{3} \left(\frac{A_1 B - A B_1}{B/d_1^2 - B_1/d^2} \right) \right]^{1/2}$$

$$c = \left[\frac{A_1 d - A B_1}{A_1/d^2 - A/d_1^2} \right]$$

Where d is the interplanar distance, $A = h^2 + hk + k^2$, $B = l^2$, and $A_1 = h_1^2 + h_1 k_1 + k_1^2$, $B_1 = l_1^2$. The crystallite size R was deduced using the prominent peaks and Sherrer's formula [14-16]:

$$R = \frac{0.9\lambda}{\beta_{1/2} \cos \theta}$$

Where $\beta_{1/2}$ is the full width at half maximum of the prominent peak.

The average grain size of the samples was determined by a(HR-TEM) of the kind JEOL JEM-2100. IR spectra were taken in the range of $200 - 2000 \text{ cm}^{-1}$ by Fourier-transform infrared spectrometer of the type Bruker Tensor 27. The magnetic hysteresis loops were recorded at room temperature by vibrating sample magnetometer

operating system v 1.6 control software Oxford OX8JTL, England (National Research Center – El Dokky). FMR measurements were performed at room temperature by **Brukeremx EPR Spectrometer located in the National Center for Radiation Research and Technology (NCRRT)**. **Note:** Some parameters of Brukeremx EPR Spectrometer were changed to be suitable for recording the ferromagnetic resonance data produced from these soft and hard magnetic samples.

3 RESULTS AND DISCUSSION

3.1 X-ray diffraction (XRD) analysis.

Fig. (1) shows the recorded XRD patterns for the prepared samples. The data obtained from XRD analysis are presented in Table (1). It is shown that the XRD pattern of the spinel MgFe_2O_4 nanoferrite has a single phase of pure cubic spinel structure as compared with JCPDS data (cards no. 01-074-2403 and 8055) and agrees with that reported previously [16]. XRD pattern of the M-type $\text{BaFe}_{12}\text{O}_{19}$ hexa-ferrite has a single phase of pure M-type hexa-nanoferrite as compared with JCPDS data (Card nos. 00-027-1029, 00-007-0276 and 01-079-1411). The X-ray diffraction pattern of the mixed ferrites shows the peaks of two phases of the cubic spinel and M-type hexaferrite [small intensities of the plans (114), (107), (116) and (205)] [17]. It is shown that the peaks of M-type hexaferrite have a relative low intensity due to its low ratio.

XRD pattern of the nanocomposite structure (the core is hexa nanoferrite coated by spinel nanoferrite as a shell) displays only the diffraction peaks of cubic spinel phase, where the peaks belonging to the core of M-type hexa-ferrite are not observed. This proves that the core material is covered completely by the cubic spinel MgFe_2O_4 nanoferrite, which confirms the successful preparation of the core-shell nanostructure. The obtained data of the lattice parameters, specific surface area (S), crystallite size (R) and strain are tabulated in Table (1).

The values of the interplanar distance d and crystallite size R of the spinel nanoferrite are, approximately, similar to that of the spinel nanoferrite of the nanocomposite structure, as presented in Table (1). The mixed material has smaller lattice constants and lower specific surface area.

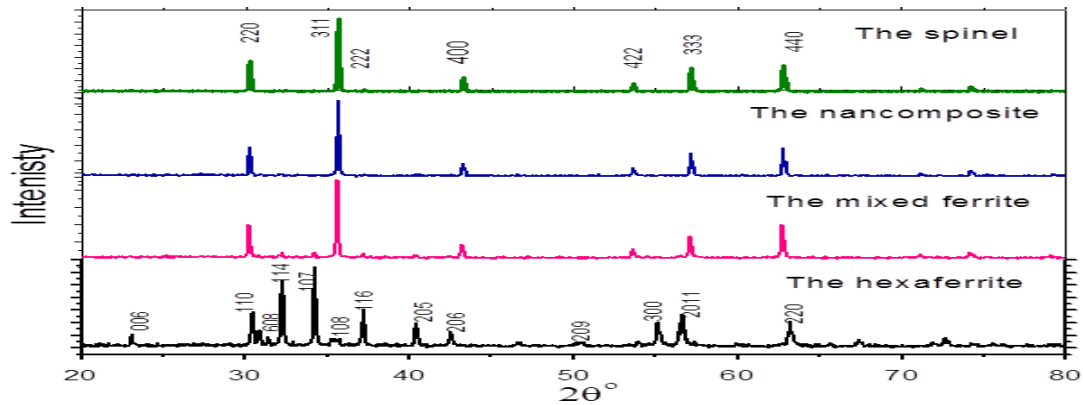


Fig.(1): XRD patterns of the prepared samples

Table (10): XRD analysis data, where d is the interplanar distance. a and c the lattice constants, R the crystallite size, S the specific surface area and strain

| Material | | Miller indices | d (Å) | a (Å) | c (Å) | R (nm) | S (m ² /g) | strain |
|-------------------------|------------------------------------|----------------|---------|---------|---------|----------|-------------------------|--------------------|
| Spinel | MgFe ₂ O ₄ | (220) | 2.963 | 8.3777 | ---- | 36.8 | 36.06 | 3*10 ⁻⁴ |
| | | (311) | 2.5262 | | | | | |
| | | (400) | 2.0942 | | | | | |
| | | (333) | 1.6123 | | | | | |
| Hexaferrite | BaFe ₁₂ O ₁₉ | (114) | 2.7372 | 5.83 | 23.38 | 32.24 | 21.6 | 6*10 ⁻⁴ |
| | | (107) | 2.5885 | | | | | |
| | | (116) | 2.3905 | | | | | |
| | | (205) | 2.2092 | | | | | |
| Mixed ferrite | spinel | (220) | 2.9546 | 8.365 | ---- | 35.975 | 36.66 | 9*10 ⁻⁴ |
| | | (311) | 2.5207 | | | | | |
| | | (400) | 2.0909 | | | | | |
| | | (333) | 1.61 | | | | | |
| | hexaferrite | (114) | 2.7781 | 4.832 | 23.357 | 29.15 | 16.18 | 8*10 ⁻⁴ |
| | | (107) | 2.6202 | | | | | |
| | | (116) | 2.4156 | | | | | |
| | | (205) | 2.2299 | | | | | |
| Nanocomposite structure | spinel | (220) | 2.9628 | 8.3766 | ---- | 36.47 | 36.38 | 6*10 ⁻⁴ |
| | | (311) | 2.5259 | | | | | |
| | | (400) | 2.0945 | | | | | |
| | | (333) | 1.6121 | | | | | |

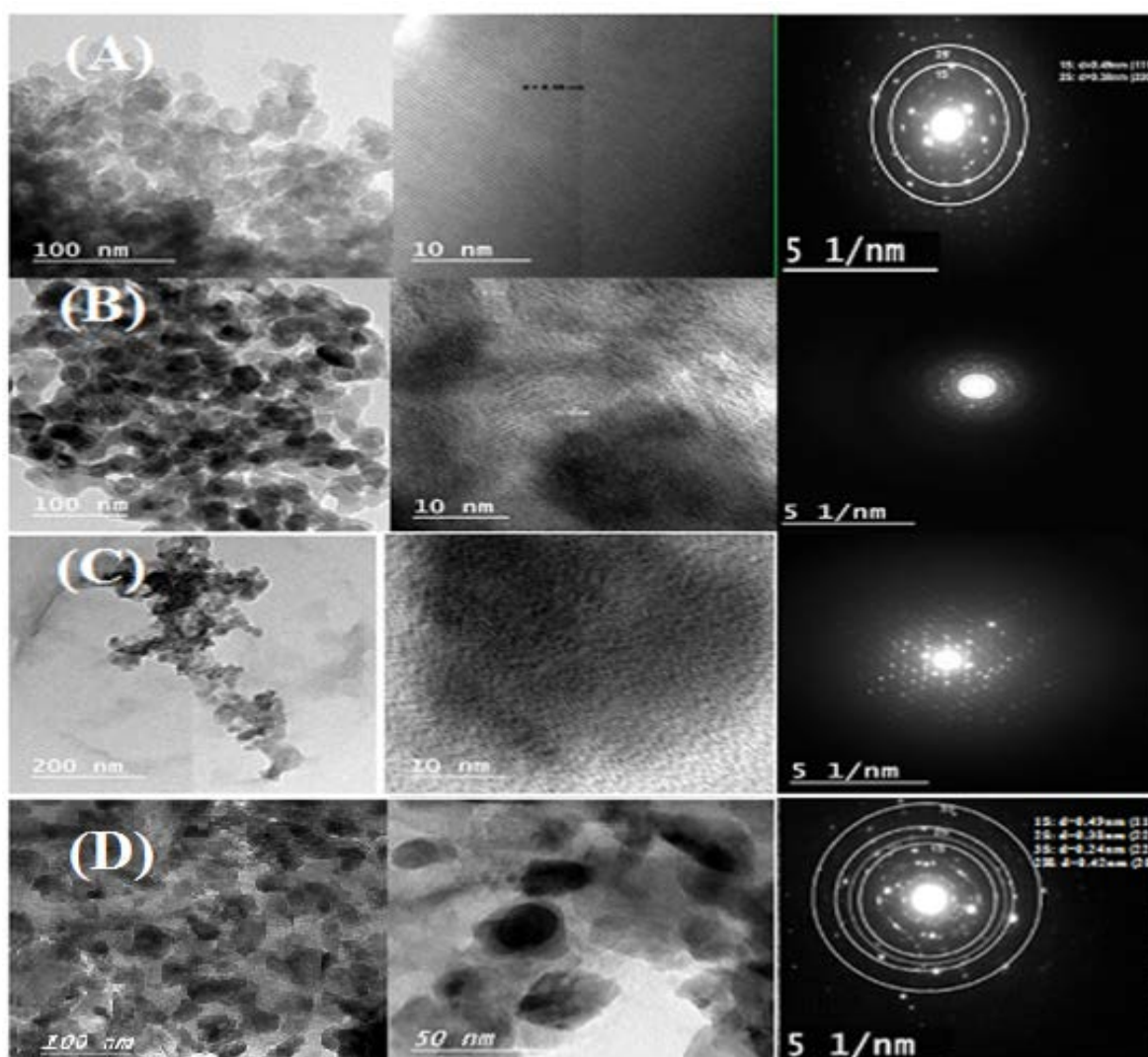


Fig. (2): HR-TEM images of (A) Spinel nanoferrites, (B) M-type hexa-nanoferrites, and (C) Mixed nanocomposites (D) nanocomposite structure

Table (2): Obtained grain size (Z) and interplanar distance (d) from HR-TEM images

| Material | Z (nm) | peak | d (Å) | Plan (hkl) |
|-------------------------|--------|------|---------|--------------|
| Spinel nanoferrite | 38.92 | 1S | 4.9 | (111) |
| | | 2S | 3.8 | (220) |
| Hexa-nanoferrite | 36.37 | 1H | 3.78 | (006) |
| Mixed nanocomposite | 44 | - | - | - |
| | | 1S | 4.9 | (111) spinel |
| Nanocomposite structure | 43.8 | 2S | 3.8 | (220) spinel |
| | | 3S | 2.4 | (222) spinel |
| | | 2H | 4.2 | (206) hexa |
| | | 3H | 4.5 | (102) hexa |

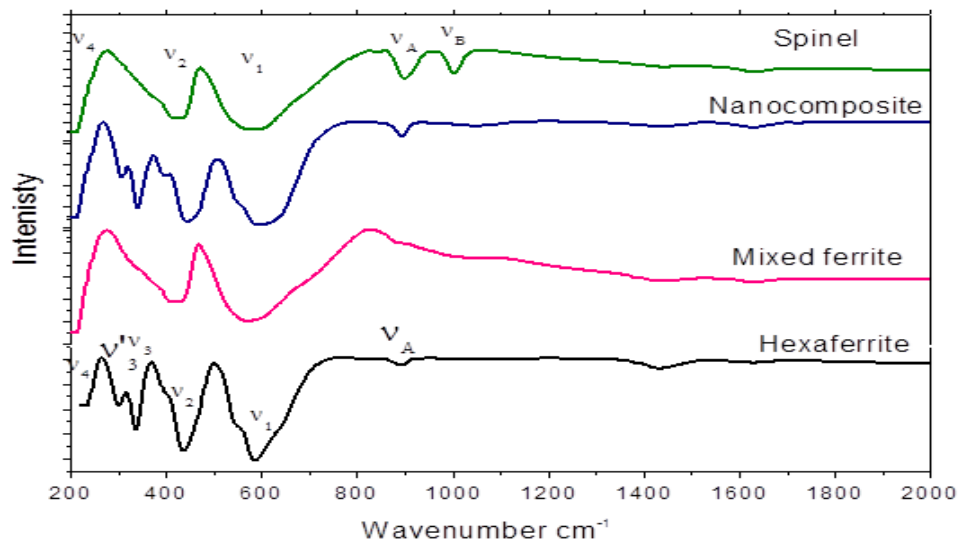


Fig.(3):FT-IR spectra for the prepared samples

Table (3): IR absorption band positions ν_n , $n = 1,2,\dots$, and ν_B , for all materials. Sh denotes shoulder

| Material | ν_1 | ν_2 | ν_3 | ν_3' | ν_4 | ν_A | ν_B |
|---------------|---------|---------|---------|----------|---------|---------|---------|
| Spinel | 580 | 434 | - | - | 215 | 900 | 1005 |
| Hexa-ferrite | 586 | 437 | 333 | 300 | 234 | 893 | - |
| Mixed ferrite | 571 | 430 | - | - | 214 | - | sh |
| Nanocomposite | 597 | 446 | 340 | 310 | 216 | 894 | 1048 |

Table (4): Obtained magnetic parameters, where M_s is the saturation magnetization, M_r the remanent magnetization, H_c the coercivity and squarness

| Material | M_s (emu/g) | M_r (emu/g) | H_c (G) | Squarness (M_r/M_s) % |
|---------------|---------------|---------------|-----------|---------------------------|
| Spinel | 18.68 | 1.36 | 14.61 | 0.073 |
| Hexa-ferrite | 63.07 | 32.57 | 5385.6 | 0.516 |
| Mixed ferrite | 26 | 5.19 | 68.76 | 0.2 |
| Nanocomposite | 22.15 | 3.3 | 55.29 | 0.15 |

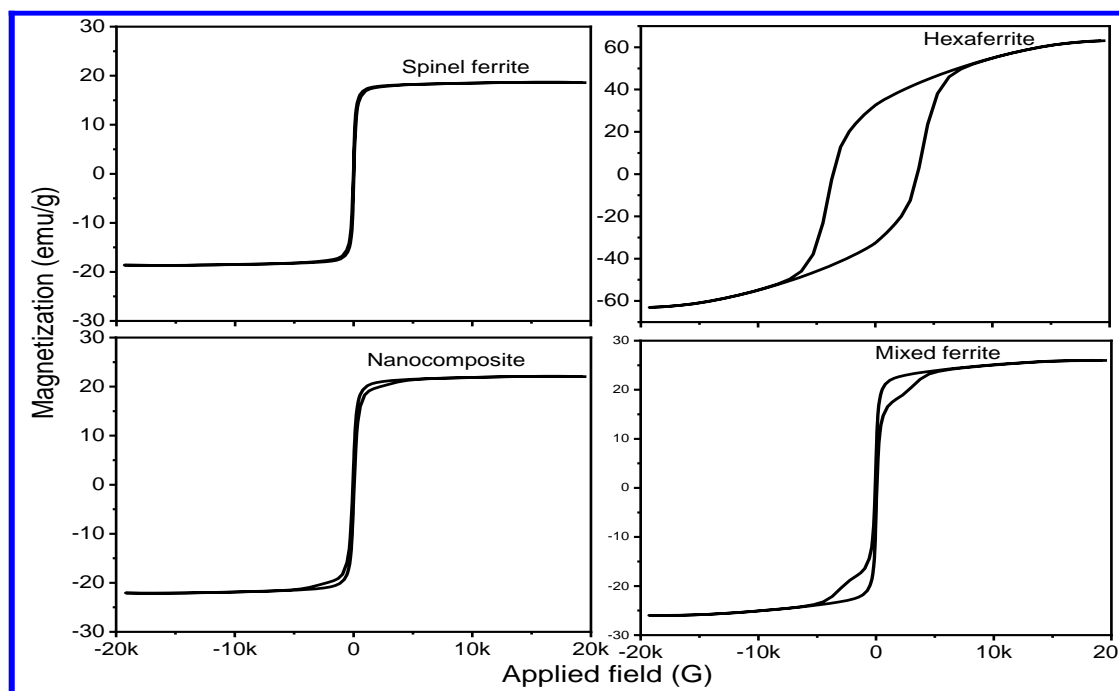


Fig. (4): Magnetic hysteresis loops of the prepared samples

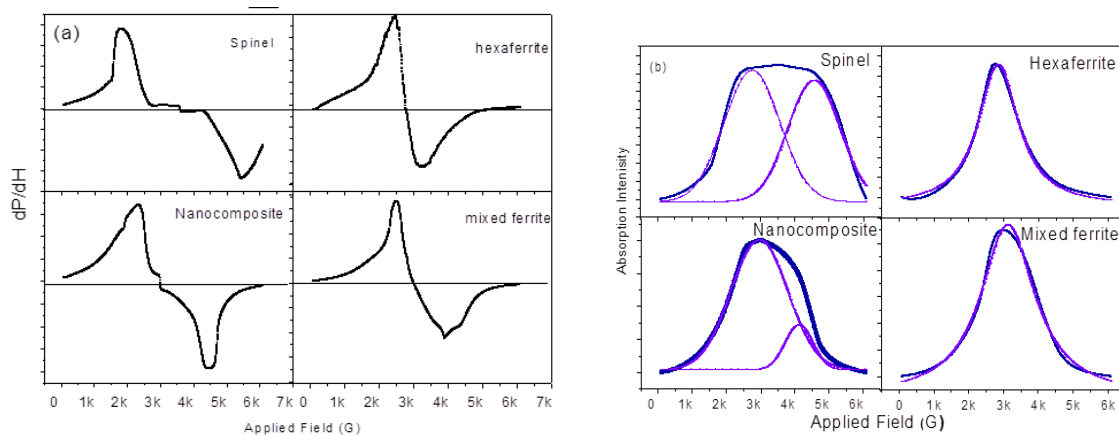


Fig (5: a): The FMR spectrum and **(b):** absorptions spectrum

Table (5): Calculated FMR parameters of different samples

| Material | Distribution | H_{r1} | ΔH_1 | H_{r2} | ΔH_2 |
|--------------------------------|--------------|----------|--------------|----------|--------------|
| Spinel nanoferrite | 2 Gaussian | 2758 | 1624 | 4563 | 1514 |
| Nanocomposite structure | 2 Gaussian | 2961 | 1668 | 4120 | 814 |
| M-type Hexa-nanoferrite | Gaussian | 2856 | 1396 | - | - |
| Mixed material | Gaussian | 3133 | 1886 | - | - |

3.2 High resolution transmission electron Microscope (HR-TEM) images

Typical HRTEM images for the samples are depicted in Fig. 2(A,B,C and D). The obtained results of the average grain sizes (Z) are given in Table (2). It is depicted that the grains of the spinel $MgFe_2O_4$ nanoferrite (Fig. 2A), M-type $BaFe_{12}O_{19}$ hexa-nanoferrite (Fig. 2B) and nanocomposite material (Fig. 2D) are agglomerated to each other due to their magnetization, where as the grains of mixed material (Fig. 2C) are granular.

Tables (2) presents that the average grain size of spinel nanoferrite is a little smaller than its crystallite size (Table 1), which may be due to the effect of material strain on XRD pattern. The average grain size of other materials is a little larger than their corresponding crystallite size. This may assign to the amorphous layer on the surface of the grains and/or the grain may exhibits more than one crystallite. The images of the nanocomposite (Fig. 2D) show darker grains where their average grain sizes are around 43.8 nm. This is a little smaller than that of mixed material (44 nm), which may be due to the disordered nature of the mixed material. The grain size of the nanocomposite is higher than its crystallite size (39.4 nm), as given in Table (2). This may be due to the fact that the crystallite size is calculated from XRD pattern of the shell material (spinel nanoferrite) which has a large strain (Table 1) and the nanocomposite structure composes of two parts the core and shell materials.

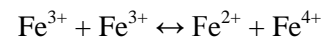
In addition, Table (2) presents that the obtained interplanar distances (d) from HR-TEM image of the nanocomposite (core-shell nanostructure) belong to the shell of spinel nanoferrite. This proves that the core material of the nanocomposite is coated completely by the spinel nanoferrite as a shell.

3.3 Infrared spectra (IR)

The recorded IR spectra for the prepared samples are shown in Fig.(3). Six absorption bands; ν_1 , ν_2 , ν_3 , ν_3' , ν_A and ν_B are observed in the nano material spectra. The data obtained from analyzing IR spectra are listed in Table (3). Appearance the three bands ν_1 , ν_2 and ν_3 in the spectrum of M-type $BaFe_{12}O_{19}$ hexa-nanoferrite confirm the formation of M-type $BaFe_{12}O_{19}$ hexa-ferrite [15, 18]. The band ν_1 may assign to the vibration of $Fe^{3+}-O^{2-}$ bond among the A-sites and ν_2 to the vibration of $Fe^{3+}-O^{2-}$ bond among the B-sites. The band ν_3 depends on the mass of the divalent metallic ions Ba^{2+}

and/or Fe^{2+} among the A-sites and is assigned to the divalent B-site metal ion-oxygen bonds [15]. Splitting the band ν_3 may be due to the presence of the divalent Ba^{2+} ions and/or Fe^{2+} ions among the B-sites.

It is seen that five absorption bands; ν_1 , ν_2 , ν_3 , ν_A and ν_B appeared in IR spectrum of the $MgFe_2O_4$ spinel ferrite proves the formation of cubic spinel structure of $MgFe_2O_4$ ferrite [6,18]. Two, relatively, high absorption bands ν_A and ν_B are observed in the spectrum, ν_A at around 900 cm^{-1} and ν_B at around 1005 cm^{-1} . The band ν_A may arise from the existence of divalent ions Mg^{2+} and/or Fe^{2+} among the A-sublattices. The broadness and higher intensity of ν_1 reveal that a hopping process arises among the tetrahedral A-sites, at the high annealing temperature, between the Fe^{3+} ions as follows:



The band ν_B may be due to existence of the tetravalent Fe^{4+} ions among the A-sites and/or oxygen trigonal distortion of the B-sites [15, 19].

The band broadness of mixed material and is similar to that of spinel ferrite may be due to the low concentration of M-type hexa-ferrite in the mixed ferrite. The absorption band ν_A is observed in all IR spectra in the range of $894-900\text{ cm}^{-1}$. It depends on the mass of the A-site divalent cations. This band is attributed to some type of lattice vibrations involving a displacement of the A-site cations [19, 20].

3.4 The magnetic measurements

The recorded room temperature magnetic hysteresis loops for the prepared samples are illustrated in Fig. (4). The magnetic parameters from analyzing the curves are given in Table (4). Fig.(4) and Table (4) illustrate that the hysteresis loop of the spinel $MgFe_2O_4$ ferrite is very narrow and has low coercivity H_c (14.61 G), saturation magnetization M_s (18.68 emu/g), remnant magnetization M_r (1.36 emu/g) and squariness M_r/M_s (0.073). This proves that this spinel nanoferrite is a soft magnetic material [6 and 18].

The hysteresis loop of M-type $BaFe_{12}O_{19}$ hexa-ferrite has the largest H_c (5.4 KG), M_s (63 emu/g), M_r (32.57 emu/g) and squariness (0.52), which proves that this material is hard magnetic material [15 and 22]. These values

agree well with that measured for bulk hexa-ferrite and the reported values in the literature [15, 20 and 22].

It is illustrated that the hysteresis loop of the mixed material sample is the overall loop of the soft and hard magnetic materials [20-24]. This sample does not exhibit a smooth hysteresis loop and shows a typical “bee waist” one that is resulted from the presence of two non-homogeneous magnetic phases in the hysteresis loop instead of a single phase. They exhibit a dual magnetic-phase phenomenon, suggesting presence of two decouples phases in the mixed ferrite material [20-24]. This indicates that the soft and hard magnetic phases are switching individually due to the incomplete exchange-coupling.

The hysteresis loop of the $Mg_{80} - H_{20}$ nanocomposite structure is similar to that of cubic spinel ferrite resulting from the presence of two homogeneous magnetic phases in the hysteresis loop illustrating a smooth single hysteresis loop. It exhibits the same M_s (22.15 emu/g) despite of its different broadness, where its M_r is 3.3 emu/g and H_c is 55.3 G. It confirms that the two different magnetic phases in the $Mg_{80} - H_{20}$ nanocomposite material are exchanged coupled to each other [10]. This proves that the nanocomposite sample presents exchange-bias field. Hence, it is believed that the horizontal broadening in this hysteresis loop is due to the exchange-bias effect [20-24]. Soft magnetic moments rotate along with the hard phase due to its external magnetic field and therefore the magnetization and demagnetization of the magnet have a single ferrimagnetic phase features [10].

Enhancing the remnant magnetization for the $Mg_{80} - H_{20}$ nanocomposite and mixed materials, as illustrated in Fig. (4) and Table (4) is mainly attributed to the overcoming of magnetic exchange interaction and high magneto-crystalline anisotropy of hard phase in competition with dipolar interaction of soft phase. Collinear arrangement of moments at the interface, leads to an enhancement of remnant magnetization [20-24]. The coercivity value of the $Mg_{80} - H_{20}$ nanocomposite and mixed materials is lower than that of pure hard phase and greater than that of pure soft phase. The mixed material has lower exchange force than that of the $Mg_{80} - H_{20}$ nanocomposite sample. Thus, the dipolar interaction among soft magnetic moments in

mixed sample becomes significant and causes a higher coercive field than that in the $Mg_{80} - H_{20}$ nanocomposite sample. So, the reverse domains in the $Mg_{80} - H_{20}$ nanocomposite structure with low nucleation field could be nucleated easily. In addition, the interface area between the soft grain boundaries and hard grains in the $Mg_{80} - H_{20}$ nanocomposite structure is larger than that in the mixed sample, therefore neighboring cladding grains would cause additional demagnetizing field and result in the reduction of overall coercivity of the $Mg_{80} - H_{20}$ nanocomposite material as compared to the mixed material [20-24].

3.5 FMR study:

The ferromagnetic resonance line width (ΔH) of ferrites depends on the random orientation of grains anisotropy and the demagnetized field induced by porosity. The (ΔH) of ferrite is the sum of three contributions [25]

$$\Delta H = \Delta H_a + \Delta H_p + \Delta H_i$$

Where:

ΔH_i represents small intrinsic linewidth (few Oersted) considered in nanoparticle material and can be ignored in polycrystalline ferrites. Moreover, ΔH_a and ΔH_p are the magnetocrystalline anisotropy and porosity induced line broadening contributions, respectively [26].

$$\Delta H_a = \frac{8\pi\sqrt{3}}{21} \frac{H_a^2}{4\pi M_s}$$

$$\Delta H_p = \frac{8}{\pi\sqrt{3}} 4\pi M_s \times P$$

Where:

M_s is saturation magnetization, H_a is the anisotropy field ($H_a = \frac{K}{M_s}$), K is the anisotropy constant and P the porosity. In large anisotropy field (relatively low saturation magnetization M_s) the resonance curve is a broad and the line width depends on anisotropy field and porosity. On the other hand, when the saturation magnetization becomes large the anisotropy field becomes small and the contribution to the line width comes only from porosity. In this case the resonance curve is narrow [27].

he FMR spectrum of spinel ferrite and nanocomposite materials have broad shoulder at low-field side (see Fig 5-a and b) which have been

seen before as FMR spectra of silica glass doped by metallic impurities [28]. This suggests that the agglomeration of MgFe_2O_4 clads (see Fig2-A and D) resulting in a similar behavior as silica glass. The absorption spectra of these two samples show broad absorption curve. The broad behavior means co-existence of multi-magnetic inhomogeneity structure. The best fit of these samples is a combination of two Gaussian lines. The fitted lines are marked as dash-dotted lines in Fig. 5(a and b) and the fitted parameters are recorded in Table (5). Neglecting the intrinsic line width ΔH_i hence, porosity and anisotropy may play the important role in changing ΔH . The close to gather values of fitting parameters of peak1 of these two samples may be returned to anisotropy field which agrees with the equal values of saturation magnetizations.

The coating M type hexaferrite by spinel ferrite makes porosity of spinel decreases from 0.67 to 0.35 (see Table 1). This may be interpreting the decreasing of ΔH values of peak2 of Gaussian fitting. The absorption spectra of M type hexaferrite and the mixed material show narrow absorption curves as shown in Fig 5(c and d). In these figures the single Gaussian fitted lines for these samples are marked as dash-dotted lines and the fitted parameters are shown in Table (5). The line width of the latter is greater than that of the former. The increase of ΔH may be due to the decrease of saturation magnetization from 63.07e.m.u/gm of the former to 22.15e.m.u/gm of the latter (see Table 4) suggesting that the anisotropy field plays non neglect role in line width.

Comparing the FMR behavior of the nanocomposite and the mixed materials, the resonance field H_r of nanocomposite is lower than that of the mixture. This may be attributed to the effect of spring exchange coupling in the nanocomposite sample. The spring exchange coupling reduces the magnetic dipolar interactions among the fine clusters and this could make ΔH of the nanocomposite more broad [25].

Conclusions

1- The attempt of building a nanocomposite structure of M-type $\text{BaFe}_{12}\text{O}_{19}$ hexagonal ferrite as a core coated by spinel MgFe_2O_4 nanoferrite as a shell has succeeded.

2- The materials were synthesized using the wet-chemical coprecipitation method and examined by XRD, HR-TEM and FT-IR spectroscopy. The as-prepared spinel and M-type hexaferrites, their mixed ferrite and nanocomposite structure were annealed at 1200 °C for 6 hours in the normal atmosphere.

3- This study proved the success of preparing the suggested nanostructure where the results obtained from FMR spectra and magnetic hysteresis loops revealed the formation of this nanocomposite structure

References

- [1] M. Awawdeh, I. Bsoul, S.H. Mahmood, J. Alloys Compd. 585 (2014) 465–473.
- [2] S. Modak, M. Ammar, F. Mazaleyrat, S. Das, P.K. Chakrabarti, J. Alloys Compd. 473 (2009) 15–19.
- [3] Amitava Moitra, Sungho Kim, Seong-Gon Kim, S.C. Erwin, Yang-Ki Hong, Jihoon Park, Comput. Cond. Matter 1 (2014) 45-50.
- [4] R.K. Kotnala, Jyoti Shah, Bhikham Singh, Harikishan, Sukhvir Singh, S.K. Dhawan, A. Sengupta, Sens. Actuat. B 129 (2008) 909–914.
- [5] Warren B. Cross, Louise Affleck, Maxim V. Kuznetsov, Ivan P. Parkin and Quentin A. Pankhurst, J. Mater. Chem. 9 (1999) 2545-2552.
- [6] M.A. Amer, T. Meaz, M. Yehia, S.S. Attalah, F. Fakhry, J. Alloys Compd. 633 (2015) 448–455.
- [7] M.A. Radmanesh, S.A. SeyyedEbrahimi, J. Magn. Mater. 324 (2012) 3094–3098.
- [8] D. Roy, C. Shivakumara, P.S. Anil Kumar, J. Magn. Mater. 321 (2009) L11–L14.
- [9] G. C. P. Leite, E.F. Chagas, R. Pereira, R.J. Prado, A.J. Terezo, M. Alzamora, E. Baggio-Saitovitch, J. Magn. Mater. 324 (2012) 2711–2716.
- [10] Soares J.M., Galdino V.B., A. Machado F.L., J. Magn. Mater. 350 (2014) 69–72.
- [11] K. Jalaiah, K. VijayaBabu, [Journal of Magnetism and Magnetic Materials, Volume 423](#), 1 February 2017, Pages 275-280.
- [12] O.M. Hemed, Journal of Magnetism and Magnetic Materials 251 (2002) 50–60.

- [13] Wei Ning, Xiang-Qun Zhang, Zhao-Hua Cheng, Young Sun, *Journal of Magnetism and Magnetic Materials* 321 (2009) 1159–1162.
- [14] B.D. Cullity, “Elements of X-Ray Diffraction“, second ed., Addison-Wesley Publishing Company, INC, United States of America, Congress catalog No 56-10137, 1978.
- [15] M.A. Amer, T.M. Meaz, S.S. Attalah, A.I. Ghoneim, *Mater. Sci. Semicond. Process.* 40 (2015) 374–382.
- [16] A. Pradeep, G. Chandrasekaran, *Materials Letters* 60 (2006) 371 – 374.
- [17] R.E. El Shater, E.H. El-Ghazzawy, M.K. El-Nimr, *Journal of Alloys and Compounds* 739 (2018) 327e334.
- [18] M.A. Amer, T. Meaz, S. Attalah, F.Fakhry, J. *Magn. Magn. Mater.* 401 (2016) 150–158.
- [19] M.A. Amer, T.M. Meaz, A.G. Mostafa, H.F. El-Ghazally, *Mater. Sci. Semicond. Process.* 32 (2015) 68.
- [20] D.H. Bobade, S.M. Rathod, M.L. Mane, *Physica B* 407 (2012) 3700.
- [21] Yan Wang, Ying Huang, Qiufen Wang, J. *Magn. Magn. Mater* 324 (2012) 3024–3028.
- [22] Kajal K. Mallick, Philip Shepherd, Roger J. Green, J. *Magn. Magn. Mater.* 312 (2007) 418–429.
- [23] ShahabTorkian, Ali Ghasemi, Reza ShojaRazavi, J. *Magn. Magn. Mater.* 416 (2016) 408–416.
- [24] G.C.P. Leite, E.F. Chagas, R. Pereira, R.J. Prado, A.J. Terezo, M. Alzamora, E. Baggio-Saitovitch, J. *Magn. Magn. Mater.* 324 (2012) 2711–2716.
- [25] C. T. Hseih, W. L. Hung, J. T. Lue, *Journal of Physics and Chemistry of Solids* 63 (2002) 733–741.
- [26] M.A. Amer , T.M. Meaz, A. Hashhash, S.S. Attalah, A.I. Ghoneim, *Materials Chemistry and Physics* 162 (2015) 442e451.
- [27] E. Schloemarn, *J. Phys. Chem. Solids* 6 (1958) 257.
- [28] [28] L.D. Bogomolova , N.A. Krasil_nikova, V.V. Tarasova, *Journal of Non-Crystalline Solids* 319 (2003) 225–231.